Available online at www.sciencedirect.com
SCIENCE DIRECT®
Respiratory Physiology & Neurobiology 145 (2005) 279–293
RESPIRATORY PHYSIOLOGY & NEUROBIOLOGY
www.elsevier.com/locate/resphysiol

Diffusional screening in real 3D human acini—a theoretical study

M. Felici[a], M. Filoche[a,b,*], C. Straus[c,d], T. Similowski[c,e], B. Sapoval[a,b]

[a] *CNRS/PMC, Laboratoire de Physique de la Matière Condensée, Ecole Polytechnique, 91128 Palaiseau, France*
[b] *Centre de Mathématiques et Leurs Applications, Ecole Normale Supérieure de Cachan, 94235 Cachan, France*
[c] *Unité Propre de Recherche de l'Enseignement Supérieur EA 2397, Université Paris VI Pierre et Marie Curie, Paris, France*
[d] *Service Central des Explorations Fonctionnelles Respiratoires, Groupe Hospitalier Pitié-Salpêtrière, Assistance Publique-Hôpitaux de Paris, Paris, France*
[e] *Service de Pneumologie et Réanimation, Groupe Hospitalier Pitié-Salpêtrière, Assistance Publique-Hôpitaux de Paris, Paris, France*

Received 30 September 2004; received in revised form 30 September 2004; accepted 20 October 2004

Abstract

Gas exchange at the acinar level involves several physico-chemical phenomena within a complex geometry. A gas transport model, which takes into account both the diffusion into the acinus and the diffusion across the alveolar membrane, is used to understand gas mixing in realistic systems. It is first shown that the behaviour of the system, computed on model geometries in 3D, only depends on the topological structure of the acinus. Taking advantage of this property, a new efficient method based on random walks on a lattice is used to compute gas diffusion in structures taken from *real* morphological data. This approach shows that, at rest, the human acinus efficiency is only 30–40%. These results provide a new evidence of the existence of diffusional screening at the acinar level. This implies permanent spatial inhomogeneity of oxygen and carbon dioxide partial pressure. The notion of an "alveolar gas" is reinterpreted as a spatial average of the gas distribution. This model casts new light on the respiratory properties of other gas mixtures, such as helium–oxygen.

Keywords: Gas mixing; Diffusion limitation; Gas exchange; Acinus; Alveolar gas; He–O_2 breathing

1. Introduction

The physiology of gas exchange in the pulmonary acinus remains a challenging issue, as it involves various physico-chemical phenomena within a complex geometry. For instance, in the distal regions of the lung, oxygen is transported towards the alveolar membrane both by convection and by molecular diffusion. Oxygen then diffuses through the tissue membrane into the blood, where it is bound by hemoglobin. Several physical parameters govern oxygen uptake at the acinar level, such as air velocity in the near-to-terminal airways, the diffusion coefficient of oxygen in air, the alveolar membrane permeability, the blood hemoglobin content and its reaction rate with oxygen. Reciprocally, carbon dioxide is discharged from the blood to the alveolar gas

* Corresponding author. Tel.: +33 1 69 33 46 52; fax: +33 1 69 33 30 04.
E-mail address: marcel.filoche@polytechnique.fr (M. Filoche).

1569-9048/$ – see front matter © 2004 Published by Elsevier B.V.
doi:10.1016/j.resp.2004.10.012

through diffusion across the membrane. It then diffuses to the zone where convection becomes dominant, and is lastly expelled from the lung. In all these processes, the morphology of the system plays an essential role. This paper focuses on the diffusive phase of acinar gas transfer. In particular, it shows how the physics of diffusion in a complex geometry can lead to important partial pressure inhomogeneities in the alveolar gas. Such inhomogeneities have strong physiological implications, notably the need for vascular regulation at the acinar level in order to match perfusion to diffusion, thus complementing the matching of perfusion to ventilation which operates on a larger geometrical scale.

Lacking direct measurements of the distribution of oxygen (or carbon dioxide) concentration in the acinus, several mathematical models have been developed and studied by numerical simulations. The aim of these models was to evaluate the simplest description, that of a uniform mixture, *the alveolar gas*. In an early model, incomplete intrapulmonary gas mixing was assigned to the finite diffusivity of oxygen, preventing it to spread evenly in the acinus within an inspiration (Scheid and Piiper, 1980). In this frame, the possible non-uniformity of the oxygen concentration was called *stratification*.

Later on, the respective roles of convection and diffusion in the gas mixing process were examined through numerical simulations (Paiva and Engel, 1985, 1987; Dutrieue et al., 2000; Tawhai and Hunter, 2001). These studies showed that concentration gradients may exist as a consequence of efficient capture of oxygen by hemoglobin, the permeability of the alveolar membrane being considered as infinite.

More recently, it has been shown that, even for an infinite capture rate of oxygen by hemoglobin, the finite membrane permeability plays a dominant role in the effective properties of the acinus (Sapoval et al., 2002a). Not only concentration gradients persist after an infinite time, but also the morphometry of the acinus is directly related to the value of the membrane permeability.

The existence of concentration gradients is due to the phenomenon known as *diffusional screening*. Diffusional screening (sometimes referred as diffusional limitation), means that O_2 molecules entering the diffusion unit (the subacinus) have a large probability to hit the surface of the alveolar membrane near the entrance than in the more distal regions. If the membrane permeability is large, O_2 molecules are absorbed at the very first hits. As a consequence, part of the surface is not active for absorption (Sapoval et al., 2002a; Felici et al., 2003). Note that the existence of concentration gradients in the acinus, due to the serial arrangement of alveoli along the pathways, was suggested by Weibel (1984).

Even in a simplified model of the acinus geometry, computing the effects of screening in 3D by solving the diffusion equation through finite elements techniques would require a mesh of at least several hundred thousands points, and more likely several million points. In this paper, we show that screening effects can however be accurately evaluated by using a new method (lattice random walk), since the diffusion process primarily depends on the branching pattern, or skeleton topology, of the acinus.

More precisely, in a first step, we show that in a 3D branched geometry, the mathematical model introduced by Sapoval et al. (2001) is equivalent to a random walk simulation on the same topological structure (Felici et al., 2004) (this approach is currently called a renormalization method in statistical physics). The equivalence only needs a calibration step which can be performed by comparing complete numerical solutions of the diffusion problem with its equivalent random walk formulation. This calibration can be realized on systems of similar geometrical complexity but of smaller sizes. The prototype geometry chosen for this procedure is a model acinus proposed by Kitaoka et al. (2000), which can be implemented in different sizes.

Once this calibration done, the real (large) system behaviour can be recovered by simulations on a tree-like lattice that reproduces the acinus morphology. This allows to easily perform simulations on large three-dimensional systems that could not be considered otherwise. Moreover, this method can be used to compute the efficiency of real human acini by considering branched lattices *designed from real morphologies*.

Fig. 1 summarizes our approach. A real human acinus is shown in Fig. 1a. This complex morphology has been modelized by Kitaoka et al. (2000) as a space-filling 3D branching structure, as shown in Fig. 1b. Fig. 1c and Fig. 1d show the branching patterns (or topologies) of the real system (Haefeli-Bleuer and Weibel, 1988) and of Kitaoka's model of same size. To calibrate the random walk method or "skeleton

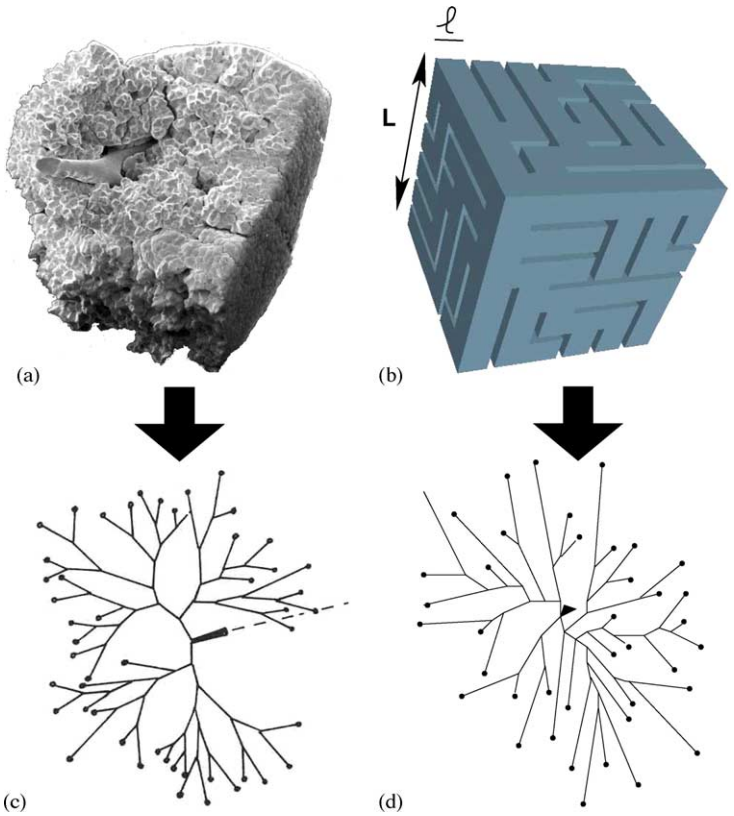

Fig. 1. (a) Silicon cast of a human pulmonary acinus (courtesy of E.R. Weibel). (b) Example of a 3D Kitaoka model of a human subacinus. In this model, each elementary cubic unit represents an alveolated duct decorated with eight alveolae. It has a size $\ell = 0.5$ mm corresponding to two alveola diameters. The overall size of the model that would correspond to a human 1/8-subacinus is thus $L = 6\ell$. (c) Branched pattern of a human subacinus (Haefeli-Bleuer and Weibel, 1988). (d) Branched pattern of the Kitaoka geometry shown in (b).

method", we apply it to Kitaoka geometries of smaller sizes and compare it with the complete numerical solution of the diffusion problem, which can be performed for these small systems. After this calibration, we then apply the skeleton method to real human acini by using the branching patterns recorded in literature.

2. Methods

2.1. The mathematical description of the oxygen transport in the acinus

We consider a simplified mathematical description of the oxygen partial pressure distribution in the acinus, introduced by Sapoval et al. (2002a). Due to the rapid decrease of the convection velocity in the branched structure of the acinus, the transition from convective to diffusive transport can be considered as abrupt. At rest, it occurs at the 1/8-subacinus entry (Haefeli-Bleuer and Weibel, 1988). In our model, the only transport mechanism for oxygen in the most peripheral airways is then molecular diffusion. The oxygen partial pressure inside the subacinus, $P_{O_2}(\vec{x})$, obeys the diffusion equation. In the stationary state, this reads: $\nabla^2 P_{O_2}(\vec{x}) = 0$, where ∇^2 represents the Laplace operator. The source of diffusion is set at the entry of the subacinus; this means that, at the entry, the oxygen partial pressure is equal to a constant value, $P_{O_2}^{entry}$. The oxygen current density $\vec{J}$ inside the acinar volume is given by Fick's law:

$$\vec{J} = -D_{O_2}\vec{\nabla}C_{O_2}(\vec{x}) \quad (1)$$

where D_{O_2} is the diffusion coefficient of oxygen in air, $C_{O_2}(\vec{x})$ is the oxygen concentration (concentration

and partial pressure only differ by a constant factor $k = 0.58 \times 10^{-7}$ mol cm^{-3} mmHg^{-1}), and $\vec{\nabla}$ is the gradient operator.

The oxygen partial pressure in the blood, $P_{O_2}^{blood}$, depends in a non-trivial way on the reactivity of hemoglobin and the partial pressure distribution in the acinus $P_{O_2}(\vec{x})$. As a first approximation, we consider $P_{O_2}^{blood}$ as constant. Let us define $\tilde{P}_{O_2}(\vec{x})$ as the difference between oxygen partial pressure in alveolar air and in blood: $\tilde{P}_{O_2}(\vec{x}) = (P_{O_2}(\vec{x}) - P_{O_2}^{blood})$, with $P_{O_2}^{blood}$ constant. The membrane permeability W_{O_2} characterizes how the diffusion current density across the membrane is related to the partial pressure difference across this membrane:

$$J = kW_{O_2}(P_{O_2}(\vec{x}) - P_{O_2}^{blood}) = kW_{O_2}\tilde{P}_{O_2}(\vec{x}) \tag{2}$$

Imposing the conservation of the current density across the membrane leads to the following boundary condition ($\vec{n}$ being the normal direction out of the alveola):

$$-D_{O_2}\frac{\partial \tilde{P}_{O_2}}{\partial n} = W_{O_2}\tilde{P}_{O_2} \tag{3}$$

The mathematical model therefore is constituted of the following set of equations (Laplace equation and boundary conditions):

$$\begin{cases} \nabla^2 \tilde{P}_{O_2} = 0 & \text{inside the acinus} \\ \dfrac{\partial \tilde{P}_{O_2}}{\partial n} = -\dfrac{1}{\Lambda_{O_2}}\tilde{P}_{O_2} & \text{at the alveolar surface} \\ \tilde{P}_{O_2} = \tilde{P}_{O_2}^{entry} & \text{at the acinus entrance} \end{cases} \tag{4}$$

with $\tilde{P}_{O_2}^{entry}$ defined as:

$$\tilde{P}_{O_2}^{entry} = P_{O_2}^{entry} - P_{O_2}^{blood} \tag{5}$$

The parameter Λ_{O_2} in Eq. (4), defined as the ratio of the diffusion coefficient of oxygen in air to the membrane permeability with respect to oxygen, $\Lambda_{O_2} \equiv D_{O_2}/W_{O_2}$, is called the *unscreened perimeter length* or the *exploration perimeter* for oxygen. This parameter plays an important role in the gas exchange process because, depending on its value, diffusional screening may or may not occur for a given system geometry.

For an acinus of total surface area S and overall diameter L, the surface conductance is $W_{O_2}S$, whereas the diffusional conductance to reach the surface is of order $D_{O_2}L$. When the two are equal, the length Λ_{O_2} is equal to S/L, L being the subacinus diameter. This ratio, called the *surface perimeter* and denoted by L_p, corresponds to the average length of a planar cut of the alveolar surface. For Kitaoka's geometries of size L, the surface perimeter L_p is of order $8(L/\ell)^2\ell$ as each cubic elementary unit contains 8 alveolae, each of perimeter length ℓ.

The fact that the purely physico-chemical length Λ_{O_2} is related to acinus morphological dimensions introduced the notion that screening could play a role in mammal's respiration (Sapoval, 1994). If the acinus perimeter were too large, then the conductance would be dominated by diffusion effects and a large part of the surface would be inactive. This is the reason why the lungs have to be divided in a large number of small acini (Sapoval et al., 2001, 2002b). Actually, whatever their size, *all mammalian acini perimeters are of order* Λ_{O_2} (between 15 and 30 cm). In the human lung, the physical length Λ_{O_2} is around 28 cm and the morphometrical data on human acini give: $L_p \simeq S/L \simeq 30$ cm. These two lengths are very close indicating that screening is a critical issue for the human respiration (Sapoval et al., 2002a).

The flux across the alveolar membrane is given by:

$$\Phi = \int_{\text{acinar surface}} kW_{O_2}\tilde{P}_{O_2}(\vec{x})\,dS \tag{6}$$

In order to quantitatively measure the diffusional screening, one can define a system efficiency η, as the ratio of the real flux to the ideal flux obtained if no screening effects were present (infinite diffusivity or infinite Λ):

$$\eta(\Lambda_{O_2}) = \frac{\int_{\text{acinar surface}} W_{O_2}\tilde{P}_{O_2}\,dS}{W_{O_2}\tilde{P}_{O_2}^{entry}S} \tag{7}$$

This quantity is used to measure the fraction of the surface that is really active. It depends only on the unscreened perimeter length and on the geometry of the system. For this reason, we explicitly indicate the dependence on Λ_{O_2} by putting $\eta = \eta(\Lambda_{O_2})$. As defined, the efficiency measures the fraction of the acinar surface that is really active for gas exchange. It is an important quantity, as it affects the total oxygen uptake in the lung. Indeed, assuming that all acini are identical, the total oxygen flux in the lung can be written as:

$$\Phi_{lung} = kN_{ac}\eta(\Lambda_{O_2})W_{O_2}\tilde{P}_{O_2}^{entry}S \tag{8}$$

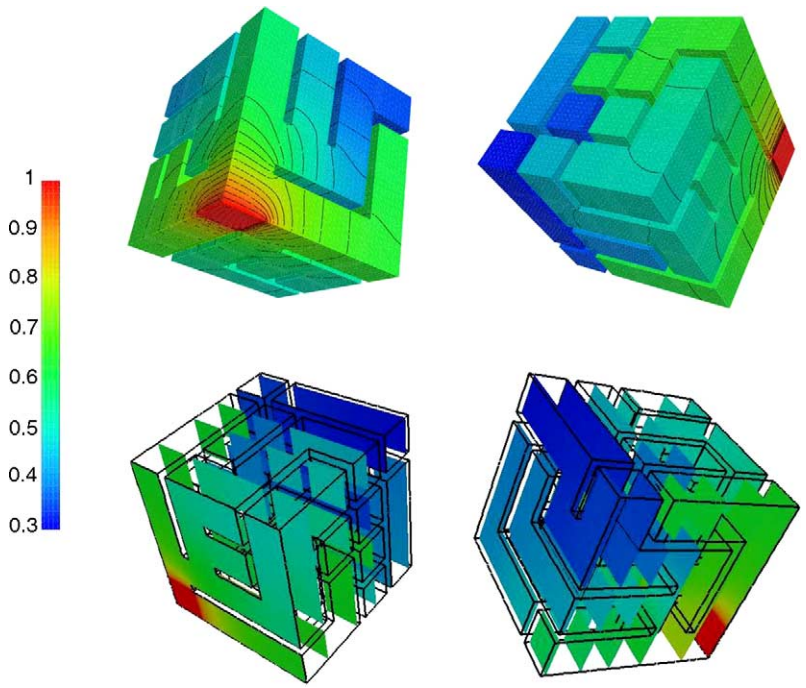

Fig. 2. Different views of oxygen partial pressure in the 3D Kitaoka model for $L = 4\ell$ and for an unscreened perimeter length $\Lambda_{O_2} = 256\ell$. Top: oxygen partial pressure is plotted in colour. Black lines are isolevels of the partial pressure. Bottom: oxygen partial pressure in different planes within the 3D model.

where N_{ac} is the total number of acini in the lung and k is the above defined constant relating concentration and partial pressure. Now, the product of N_{ac} by S is the total alveolar surface area in the lung, S_{lung}. So, besides the physical parameter W_{O_2}, the total flux is directly proportional to the alveolar surface area and to the acinus efficiency $\eta(\Lambda_{O_2})$.

Note that, since the efficiency grows with unscreened perimeter length, it decreases with permeability. The global flux depends then on the permeability of the membrane in a non-trivial way. This is important for the case of carbon dioxide, to be discussed further, which behaves very differently from oxygen, as the permeability of the acinar membrane for carbon dioxide is 20 times higher than for oxygen.

2.2. Solution of the problem in a model 3D geometry

We have applied the mathematical description given by Eq. (4) to a three-dimensional Kitaoka model acinus (Kitaoka et al., 2000). Kitaoka's algorithm generates intra-acinar pathways in a semi-stochastic way. The resulting three-dimensional labyrinths show a mostly dichotomous branched structure with space-filling properties. The acinar volume is schematized as a cube of side L, the alveolar ducts having a constant square section of side ℓ. To obtain the human 1/8-subacinus, as described by Haefeli-Bleuer and Weibel (1988), one must take $L = 3$ mm and $\ell = 0.5$ mm, hence $L = 6\ell$ (see Fig. 1b).

Eq. (4) is solved through the finite elements method (FEM) on tetrahedral meshes. For this, a FEM solver in C has been written, whereas the meshes are generated by the commercial software SIMAIL.[1] Unfortunately, the human subacinus is too large for this computation: a sufficiently refined mesh (tetrahedron side of the order of $\ell/20$) would require millions of points. Still, a complete numerical solution can be computed for Kitaoka geometries of size $L = 3\ell$ and $L = 4\ell$.

The oxygen partial pressure in a Kitaoka acinus of size $L = 4\ell$ and surface perimeter $L_p \simeq 128\ell$ (see ear-

[1] Software SIMAIL, Company SIMULOG, http://www.simulog.fr.

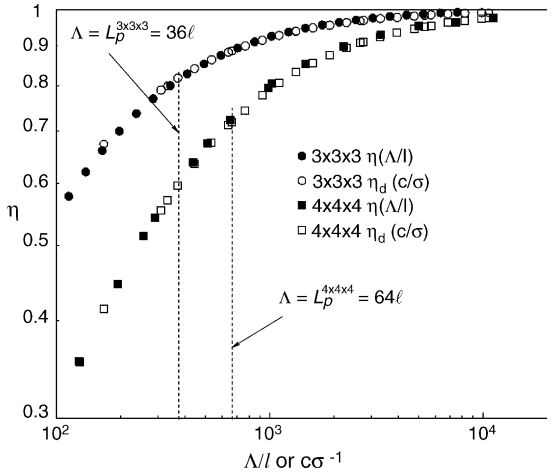

Fig. 3. The efficiency η as a function of the unscreened perimeter length Λ for Kitaoka 3D models, for $L = 3\ell$ and $L_p \approx 72\ell$ (circles) and $L = 4\ell$ and $L_p \approx 128\ell$ (squares). Filled symbols: direct numerical solution of the mathematical model; open symbols: solution η_d by the skeleton method after calibration.

lier) is shown in Fig. 2 for an unscreened perimeter length $\Lambda_{O_2} = 256\ell$. As one can see, the oxygen partial pressure is far from uniform. In this case, the efficiency η is 51%.

A plot of the efficiency $\eta(\Lambda_{O_2})$ is presented in Fig. 3 (filled symbols). The efficiency varies as a power law for $\Lambda_{O_2} < L_p$ and slowly approaches 1 for $\Lambda_{O_2} \gg L_p$. Note that, for a given value of Λ_{O_2}, the efficiency increases with decreasing acinus size: optimization of diffusional transport requires a small size. This result had already been asserted from numerical simulations in 2D (Felici et al., 2003) and is now confirmed for 3D systems.

2.3. The "skeleton method"

In the skeleton method, molecular diffusion is represented by random walks in a coarse-grained geometry. The skeleton of a 3D branched system can be defined as a tree with 1D branches, each branch representing an alveolar duct. Putting one site per unit distance ℓ, ℓ being the ducts diameter, one obtains a branching lattice. Fig. 4 illustrates this procedure in the case of a 2D branched system.

Molecular diffusion of oxygen is simulated by a superposition of random walks on the lattice, starting from the entry. It is known that diffusion is the result

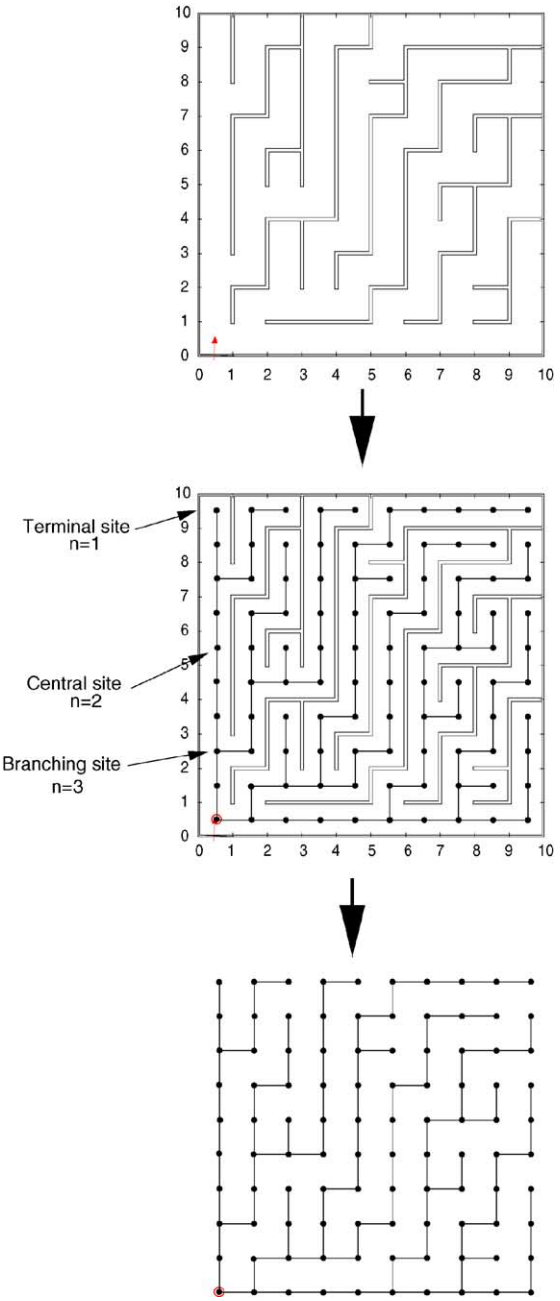

Fig. 4. Illustration of the skeleton method in 2D. Top: a bidimensional branched system (Kitaoka 2D model for $L = 10\ell$). Center: a skeleton is generated from the model. Sites are placed successively, at intervals equal to the duct diameter. For each site, one can define a coordination number n (number of lattice sites connected to the site itself). The number of absorbing walls surrounding a site is equal to $4 - n$ in 2D, and to $6 - n$ in 3D. Bottom: the 2D skeleton.

of the many collisions of molecules causing random motion in space. Thus, a great number of particles performing a random motion behave like a diffusing gas.

Absorption by the alveolar walls is included in the model. The walker moves along the tree or from site to walls, as follows: (i) one of the six directions of space (forward/backward, left/right, up/down) is chosen at random; (ii) if there is a neighbouring lattice site in this direction, the move is effective; (iii) otherwise, the walker collides with a wall site and is either absorbed with probability σ (and the walk ends) or reflected with probability $(1-\sigma)$ to its original site and the walk goes on (Fig. 4).

The average occupation number of a lattice site i, k_i, is defined as the average number of times this site has been visited by a walker. To represent the oxygen mean concentration in a site, we consider $K_i = k_i/k_0$, k_0 being the average occupation number of the entry site. The efficiency η_d of the system ("d" stands for discrete) can be defined as:

$$\eta_d = \frac{\sum_i K_i s_i}{\sum_i s_i} \tag{9}$$

2.4. Comparison between finite elements method and the skeleton method for Kitaoka's model acini

We have applied the skeleton method to the branched systems corresponding to the Kitaoka model acini of size $L = 3\ell$ and $L = 4\ell$ and computed the efficiency η_d as a function of $1/\sigma$. Using the results of finite elements simulation of the diffusion equation, we were able to calibrate the skeleton method results. One finds that the probability σ (parameter of the absorption in the skeleton method) is simply proportional to ℓ/Λ: $\ell/\Lambda = c/\sigma$, c being a constant factor found to be equal to 1.3. This number is not size sensitive and has been found to remain the same among 20 different realizations of Kitaoka's geometries. The result of the calibration is shown in Fig. 3 where η is plotted in filled and η_d in open symbols.

The skeleton method allows then to obtain good quantitative results through much simpler and faster numerical simulations than the direct computation on three-dimensional geometries. For one value of Λ, the direct computation may take around 1 hour when the random walk computation would take around 1 min. But, most importantly, this method can easily be applied to *real morphologies*, as it only requires the knowledge of their branching patterns. These patterns have been provided by the systematic studies of human acini by Haefeli-Bleuer and Weibel (1988).

3. Results

3.1. Diffusional screening in real human acini

We have considered eight examples of human subacini. The morphology was as described by Haefeli-Bleuer and Weibel (1988) (see Fig. 5). We designed the branched lattice with a lattice constant ℓ of 0.46 mm. The lengths of the alveolar ducts were rounded off to integer multiples of ℓ and the corresponding number of sites were associated to the branches. The alveolar surface of these subacini was in between $649\ell^2$ and $1193\ell^2$.

Fig. 6 is a plot of the efficiency versus the unscreened perimeter length, computed by the skeleton method. The spread of the eight curves $\eta(\Lambda)$ reflects the anatomical variability (one has to recall that η is a decreasing function of the acinar surface). For the human subacinus ($\Lambda_{O_2} = 600\ell = 30$ cm), the efficiency ranges from 20 to 40%. Average of 32% and relative variation of mean is 0.16. Screening is then effective at rest. Schematically, the acinus behaves as if only one third of its total alveolar surface was *totally* active, i.e. with the partial pressure maximal and equal to the entrance partial pressure.

The oxygen flux is proportional to the product of the efficiency by the alveolar surface area. Thus, although the relative variation in efficiency among the eight subacini is of the order 0.16, the flux variation is only of the order 0.08. The global efficiency of the acinus, i.e. the ratio of the total flux to the total surface area, is 30%.

For convenience, the efficiency may be schematically described in terms of a fraction of surface working uniformly and the remaining not working at all. But in the real system, there is a smooth distribution of partial pressure, decreasing from the entrance of the acinus to the last generations of branching. If one computes the amount of surface that is responsible for 90% of the global oxygen flux for one subacinus with $\eta = 39\%$, the result is 79% of the acinar surface. The reason is that, in a tree structure, most of the surface is generated by

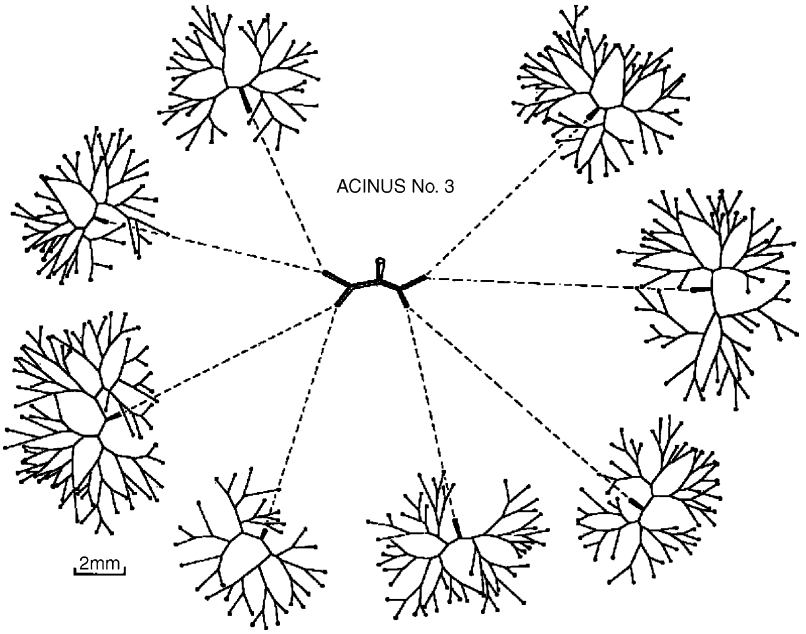

Fig. 5. Eight examples if the branching pattern of a human acinus (Haefeli-Bleuer and Weibel, 1988). The 1/8-human subacini are shown.

the last generations of branching. Their contribution to the flux is important, even though the partial pressure is reduced by screening.

The above results apply to breathing at rest. During exercise, the convection–diffusion transition occurs deeper in the subacinus because of the increase of the inlet velocity of air (Sapoval et al., 2002a). In our picture, this implies that, instead of being at the entry, the source of diffusion is located inside the acinus. The diffusive cell is then smaller—and consequently more efficient—than at rest.

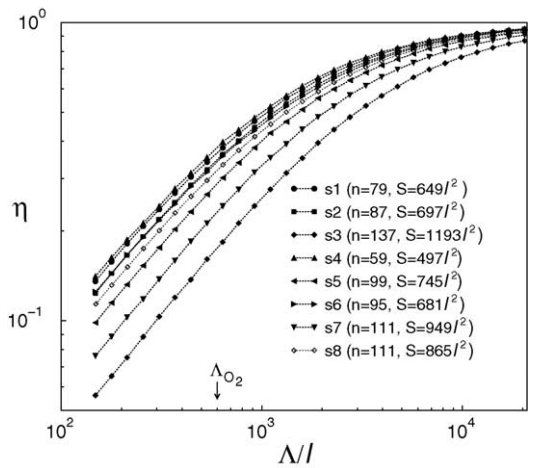

Fig. 6. Efficiency as a function of Λ for the eight branching patterns of Fig. 5 as obtained through the skeleton method. The value of Λ/ℓ in the human acinus is equal to 600.

3.2. Generalization of the model to other gas mixtures

The model presented above holds for any gas mixture. Indeed, Eqs. (4) and (5) are valid for any respiratory gas, i.e. any gas permeating the alveolar membrane. The unscreened perimeter length for a respiratory gas X is defined by:

$$\Lambda_X = \frac{D_{X,B}}{W_X} \tag{10}$$

where W_X is the permeability of the alveolar membrane for gas X and $D_{X,B}$ is the binary diffusion coefficient of the gas X in the gas mixture B. The global flux of X is:

$$\Phi_X = kW_X\eta(\Lambda_X)\tilde{P}_X^{\text{entry}}S_{\text{lung}} \tag{11}$$

It is proportional to the partial pressure difference $\tilde{P}_X^{\text{entry}} = P_X^{\text{entry}} - P_X^{\text{blood}}$ and to the product $W_X\eta(\Lambda_X)$, which is a non-trivial function of $D_{X,B}$ and W_X.

Table 1
Parameters and computed quantities for different gas mixtures in a Kitaoka model acinus of size $L = 6\ell$

	D_X[a] ($cm^2\ s^{-1}$) (data)	W_X[b] ($cm\ s^{-1}$) (data)	Λ_X (cm) (data)	$\eta(\Lambda_X)$ (simulation)	$W_X\eta(\Lambda_X)$ ($cm\ s^{-1}$) (simulation)	$\mu(\Lambda_X)$ (simulation)
O_2 in air	0.19	0.79×10^{-2}	25	0.33	0.26×10^{-2}	0.42
CO_2 in air	0.17	0.16	1.0	0.04	0.64×10^{-2}	0.06
O_2 in Heliox	0.73	0.79×10^{-2}	92	0.60	0.47×10^{-2}	0.67
CO_2 in Heliox	0.61	0.16	3.8	0.09	1.12×10^{-2}	0.12
CO_2 in O_2	0.15	0.16	0.94	0.03	0.48×10^{-2}	0.05

Heliox® is a 79% He–21% O_2 mixture.
[a] Reid et al. (1987).
[b] Weibel et al. (1993).

In this context, it is useful to define the zero-dimensional variable $u(\Lambda_X)$:

$$u(\Lambda_X) = \frac{\tilde{P}_X}{\tilde{P}_X^{\text{entry}}} \quad \text{with} \quad \tilde{P}_X = P_X - P_X^{\text{blood}} \tag{12}$$

Using this new variable in Eq. (4), one has:

$$\begin{cases} \nabla^2 u(\Lambda_X) = 0 & \text{inside the acinus} \\ \dfrac{\partial u(\Lambda_X)}{\partial n} = -\dfrac{1}{\Lambda_X} u(\Lambda_X) & \text{at the alveolar surface} \\ u(\Lambda_X) = 1 & \text{at the entry} \end{cases} \tag{13}$$

whereas Eq. (7) reads:

$$\eta(\Lambda_X) = \frac{1}{S} \int_{\text{acinar surface}} u \, \mathrm{d}S \tag{14}$$

Solving the set of Eq. (13), one finds the spatial distribution of $u(\Lambda_X)$ in the alveolar volume (see, for instance, Fig. 2). This is in general not uniform and can be strongly inhomogeneous for small Λ_X. Let us define $\mu(\Lambda_X)$ as the average value of $u(\Lambda_X)$ over the acinar volume V:

$$\mu(\Lambda_X) = \frac{1}{V} \int_{\text{acinar volume}} u \, \mathrm{d}V \tag{15}$$

Note that $\eta(\Lambda_X)$ and $\mu(\Lambda_X)$ are different as they are related to, respectively, the average flux and the average pressure.

From $\mu(\Lambda_X)$, one obtains the average partial pressure of X in the acinar volume, $\langle P_X \rangle^{\text{alv}}$, by:

$$\langle P_X \rangle^{\text{alv}} = P_X^{\text{blood}} + \mu(\Lambda_X)(P_X^{\text{entry}} - P_X^{\text{blood}}) \tag{16}$$

Eqs. (13)–(15) have been solved for oxygen and for carbon dioxide in different gas mixtures: air, Heliox® (a 21% O_2–79% He mixture) and pure oxygen. The results of simulations on one representative subacinus are presented in Table 1.

The comparison between oxygen and carbon dioxide in air is interesting. The diffusivities D in air are approximately the same for O_2 and CO_2, whereas the membrane permeability is much larger for CO_2 (ca. 20×), due to the higher solubility of carbon dioxide in aqueous solutions. As a consequence, the unscreened perimeter length Λ is smaller for CO_2 and the acinus is *much less* efficient for CO_2 clearance than for O_2 uptake. The net result is that the flux *per unit partial pressure difference* for CO_2 (proportional to $\eta(\Lambda) \times W$) is not 20 times but only 2.5 times larger than the corresponding value for O_2 (see Eq. (11)). One can note that $\mu(\Lambda)$ follows in first approximation $\eta(\Lambda)$.

The two cases are illustrated in Fig. 7. The O_2 and CO_2 partial pressure distributions in a two-dimensional Kitaoka model acinus are compared for $\Lambda_{O_2} = 800\ell$ and $\Lambda_{CO_2} = (1/20)\Lambda_{O_2}$. As one can see, the CO_2 partial pressure is uniform and maximal (i.e. at equilibrium with blood) in most of the volume, $\tilde{P}_{CO_2}$ being appreciably different from zero only near the entry.

Let us now consider the case of Heliox® in which oxygen is mixed with helium instead of nitrogen. Collisions against the lighter molecules are less efficient for scattering, so that the oxygen diffusion coefficient is larger in this mixture than in air. This increases the unscreened perimeter length, whereas the permeability remains constant. Efficiency increases by a factor of 2. Similarly, the replacement of N_2 by He favours carbon dioxide clearance (see clinical examples further).

In the case of pure oxygen breathing, diffusion screening is absent. $\tilde{P}_X$ is maximal everywhere, and oxygen uptake is increased. However, diffusion screening is present for CO_2, as the diffusion coefficient

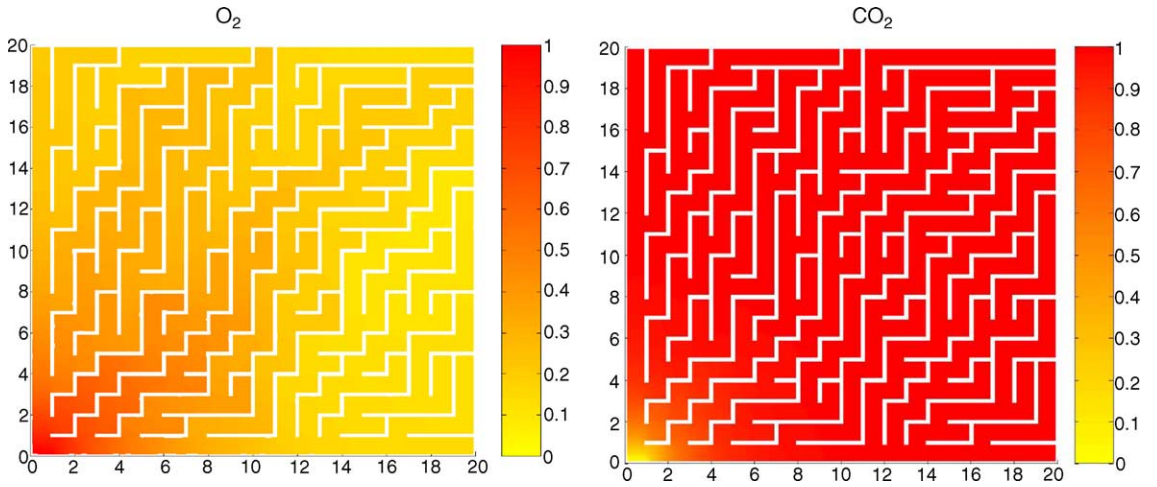

Fig. 7. Oxygen and carbon dioxide distribution in a two-dimensional Kitaoka acinus. Left: oxygen partial pressure $P_{O_2}(\vec{x})$ for $\Lambda_{O_2} = 800\ell$; right: carbon dioxide partial pressure $P_{CO_2}(\vec{x})$ for $\Lambda_{CO_2} = 40\ell$. In most of the acinus, the CO_2 partial pressure is very close to the blood CO_2 partial pressure and the flux is very small. The active region (where the gradient is different from zero) is located near the entrance (lower left corner), as for oxygen, but it is much smaller.

D_{CO_2,O_2} differs little from $D_{CO_2,air}$, and all other quantities are the same as in air.

3.3. *There is no such thing as a "uniform alveolar gas": a new physiological model for the pulmonary acinus*

In respiratory physiology, a commonly used concept is that of an "alveolar gas" characterized by uniform partial pressures of the different gases. Although the above considerations show that the distribution of oxygen and carbon dioxide are not homogeneous in the acinus, we now show that the notion of a "uniform alveolar gas" may be interpreted in terms of space averages. Indeed, the spatial average of the partial pressure over the acinar volume (obtained with Eqs. (13) and (14)), is usually close to the pressure generally accepted for the (uniform) alveolar gas.

In order to obtain the averages, one must choose values of the partial pressures at the input and output of the lung compartment. One may assume for the partial pressures at input those in the mouth: $P_{O_2}^{entry} = 150\,mmHg$ and $P_{CO_2}^{entry} = 0.3\,mmHg$. This gas is saturated with water vapour.

At the output, one must choose the blood partial pressures, which we suppose uniform. In the mixed venous blood, which is pumped by the heart to the alveoli, the CO_2 partial pressure varies between 43 and 47 mmHg: we choose the mean value $P_{CO_2}^{blood} = 45\,mmHg$. Lastly, we assume that the O_2 and CO_2 fluxes are equal, as they must be in the steady state. Using Eq. (11), this gives:

$$\frac{\tilde{P}_{O_2}^{entry}}{\tilde{P}_{CO_2}^{entry}} = \frac{W_{CO_2}\eta(\Lambda_{CO_2})}{W_{O_2}\eta(\Lambda_{O_2})} = 2.5 \tag{17}$$

Given $P_{O_2}^{entry}$, $P_{CO_2}^{entry}$ and $P_{CO_2}^{blood}$, Eq. (17) yields for $P_{O_2}^{blood}$ the value $P_{O_2}^{blood} = 38.5\,mmHg$. Remarkably, this value, obtained from a screening theory, is very close to the measured value in the mixed venous blood which is around 40 mmHg.

Using Eqs. (16) and (17), one finds: $\langle P_{O_2}\rangle^{alv} = 86\,mmHg$ and $\langle P_{CO_2}\rangle^{alv} = 42\,mmHg$. These are not far from the values generally accepted for the uniform "alveolar gas". In our model, they are averages over an inhomogeneous distribution, directly related to the existence of screening through $\mu(\Lambda_X)$.

The general agreement between the partial pressures in the two models leads us to propose a new physiological model for the acinus, in which $P_{O_2}(\vec{x})$ decreases smoothly from $P_{O_2}^{entry} = 150\,mmHg$ at the subacinus entry to a minimum of 40 mmHg in the less accessible regions of the system (Fig. 8).

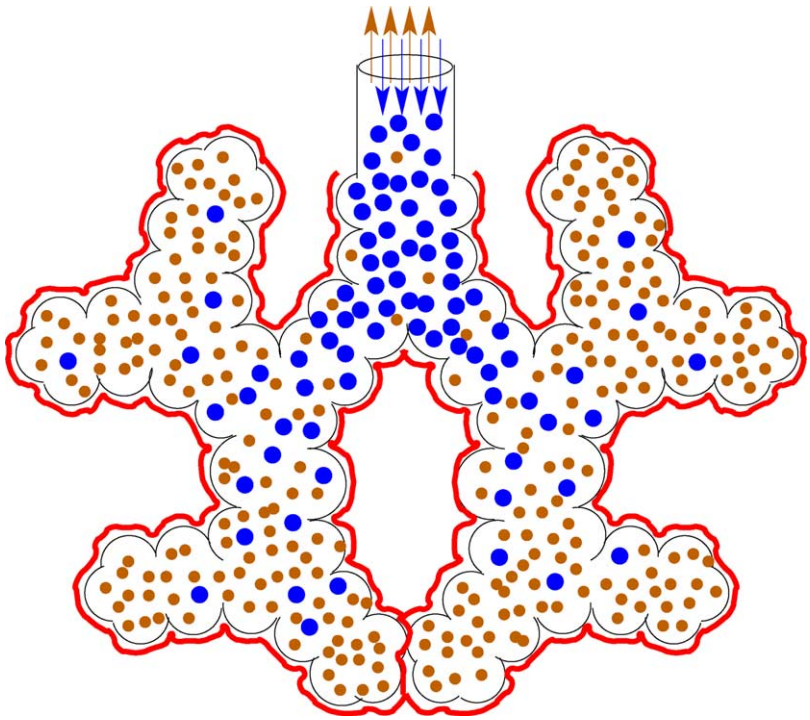

Fig. 8. Scheme of the subacinus at work. Oxygen is depicted in blue and carbon dioxide in brown. The oxygen partial pressure is maximal at the entry of the subacinus. It decreases smoothly towards the distal regions of the acinar volume, because of diffusional screening. In contrast, carbon dioxide is rather homogeneously distributed in the acinar volume except for a small region near the entry.

In spite of its simplified description, this physical model of the diffusion in the subacinus yields partial pressures and fluxes that are close to the measured values. In order to obtain more precise estimations, one should reconsider the approximations that have been made. The main approximation concerns pulmonary capillary blood, which is treated as a *uniform* and *infinite* buffer for oxygen. In particular, hemoglobin saturation is not taken into account. For this reason, the screening effect is somewhat overestimated. However, although the saturation of hemoglobin would contribute to reduce the screening effects (Keener and Sneyd, 1998), it will not cancel as was shown in a 2D Kitaoka's acinus (Felici, 2003). Furthermore, it would contribute to increase $\langle P_{O_2} \rangle^{alv}$ above 86 mmHg. In order to study these effects, one should be able to modelize the oxygen–hemoglobin binding dynamics and blood flow distribution in the acinus. Note also that the convection–diffusion transition has been dealt with in a very approximate way, as being abrupt and located at the subacinus entry.

4. Discussion

The very existence of diffusional screening at the acinar level and the corresponding intra-acinar heterogeneity in oxygen partial pressure have several possible consequences or applications, as exemplified further.

4.1. Respiratory flexibility and reserve

The suboptimal character that diffusional screening confers to the acinus as a gas exchanger can be viewed negatively. It can also be viewed as protective, providing, so to speak, a readily available "respiratory reserve". During exercise for instance, the distal displacement of the convection–diffusion transition that is due to the higher ventilatory flow decreases the magnitude of screening or even suppresses it, therefore improving acinar efficiency. Conversely, the respiratory flexibility between rest and exercise would be limited if the acini were already fully efficient at rest. This is

the case, as mentioned earlier, for small acini. In newborns, the acini are small (Osborne et al., 1983) and thus probably maximally efficient at rest. This could explain the development of cyanosis during crying, their sole form of "exercise" (understood as an increase of the oxygen demand). The same type of consideration may apply to some pathological conditions. In certain forms of pulmonary edema, the deterioration of the alveolar membrane results in a diminished permeability W_X, and thus in an increased $\eta(\Lambda_X)$. As the flux per unit partial pressure difference is proportional to $W_X\eta(\Lambda_X)$, the decrease in W_X is partially compensated by the increase in $\eta(\Lambda_X)$. This is true only if screening is present. When η approaches 1 (negligible screening), the net flux decreases and becomes directly proportional to the permeability. Screening could thus have a "protective" effect in delaying the occurrence of hypoxemia when the alveolar membrane deteriorates.

4.2. Regulation of pulmonary perfusion

Following the early work of Von Euler and Liljestrand (1946), it is now well established that acute alveolar hypoxia induces pulmonary vasoconstriction. By reducing blood flow in underventilated areas, hypoxic vasoconstriction preserves the ventilation–perfusion equilibrium (limitation of the extent of shunted territories) and thus maintains the arterial oxygen partial pressure. Several modulatory factors are known, both endogenous (for instance, the sensitivity of the pulmonary vasculature varies between species (Elliott et al., 1991)) and exogenous (e.g. carbon monoxide (Heistad and Wheeler, 1972) or hypothermia (Fan et al., 1992)). Small arteries are particularly sensitive to hypoxia. An acinar efficiency of about 30%, as computed earlier, leading to the situation depicted by Fig. 8, implies distal oxygen partial pressures within the acinus as low as 40 mmHg (see earlier). This should most certainly trigger hypoxic vasoconstriction, which would thus contribute to an acinar diffusion–perfusion matching similar to the more global ventilation–perfusion matching. Indeed, in the absence of such a local regulation, the proportion of blood not exposed to oxygen during an inspiration would be much higher than the 5% figure that is considered normal. Of note, such a diffusion–perfusion matching at the acinar level has consequences on the above calculations. Indeed, the acinar region that is subject to vasoconstriction is not available for oxygen diffusion. Hence, the ratio of the acinus total surface area S to the acinus overall diameter L, or surface perimeter (see Section 2.1), overestimates the *functional* surface perimeter actually available for diffusion, and underestimates the computed efficiency of the acinus. The effects of diffusional screening on the performance of the acinus as a gas exchanger will thus depend, in a given species and in given circumstances, on the sensitivity of the pulmonary microvasculature to hypoxia and on the efficiency of hypoxic vasoconstriction. Concerning CO_2, as the active region is located at the entrance of the subacinus (see Fig. 7), a weaker perfusion of the deeper regions would not affect the net gas flow.

In the case of Heliox®, for which the oxygen transfer efficiency is larger, one expects a more homogeneous perfusion. Also, the outflow of CO_2 in Heliox® would not be strongly modified by the diffusion–perfusion matching. For O_2–SF_6 and CO_2–SF_6, the active zone for oxygen uptake would be reduced and diffusion–perfusion matching would also be required for the saturation of hemoglobin. In the case of ventilation of pure oxygen, perfusion matching is not applicable.

4.3. Effects of the physical properties of gas mixtures on gas exchange

For physiological or therapeutic purposes, oxygen can be mixed with helium or other gases instead of nitrogen. This modifies both the viscosity of the mixture and the oxygen diffusivity. He–O_2 and SF_6–O_2 represent extremes in these terms, the viscosity increasing in the sequence He–O_2,[2] air and SF_6–O_2, whereas the diffusivity decreases. These changes interfere with diffusional screening. With helium–oxygen, the screening effect is expected to decrease, due to a larger Λ_X, itself due to a larger oxygen diffusivity. With SF_6–O_2, on the

[2] Helium–oxygen is used in clinical situations where a physiological or a clinical benefit is anticipated from the reduction of the viscosity of the inhaled gas, in order to reduce the resistive work of breathing. This is, for example, the case in tracheal stenosis, acute severe asthma, or acute respiratory failure of chronic obstructive pulmonary disease. In the latter two situations, the benefit may come not only from a reduced inspiratory resistive work of breathing, but also from a better emptying of pulmonary compartments with very slow time constants, leading to a lesser degree of dynamic hyperinflation and hence of elastic work of breathing (Jolliet et al., 2003).

contrary, the screening effect is expected to increase, due to a lower Λ_X due to a lower oxygen diffusivity. Experimental data in the literature are compatible with these predictions and therefore lend support to the reality and relevance of acinar diffusional screening. For example, Watson et al. (1987) observed, in mechanically ventilated dogs kept under *constant ventilatory conditions*, that the alveolo-arterial oxygen gradient AaO_2 was smaller during helium–oxygen ventilation than during air ventilation and SF_6–O_2 ventilation. In normal rabbits undergoing ventilation through a low bias flow oscillation system, Siddappa et al. (2003) observed that substituting a 60% helium–40% oxygen mixture to the baseline 60% nitrogen–40% oxygen mixture reduced AaO_2 by as much as 40%, at constant ventilatory pattern. In exercising horses, Erickson et al. (1995) observed an improvement in AaO_2 under helium–oxygen breathing that by far exceeded the change expected from the higher ventilation permitted at a given exercise level by the lower viscosity of the gas. In humans, similar observations have been reported by Schaeffer et al. (1999). In patients mechanically ventilated for acute severe asthma, these authors observed a decrease in AaO_2 from 216 ± 92 to 85 ± 44 mmHg when replacing nitrogen by helium in the gas mixture, without any other intervention. In a control group monitored during an equal period of time, no change was observed. In most of the earlier studies, no particular explanation was proposed for the helium-related reduction in AaO_2. Erickson et al. (1995) attributed this observation to a "more complete diffusion equilibration". All these results are compatible with acinar screening.

However, it should be noted that Buono and Maly (1996) failed to observe any helium-related improvement in AaO_2 at maximal exercise in trained athletes even though the helium–nitrogen substitution resulted in an increased minute ventilation (up to 30 l/min). During exercise, the convection–diffusion transition occurs deeper into the acinus (Sapoval et al., 2002a), so that efficiency is maximized and therefore becomes unresponsive to helium. In this view, the discrepancy between humans at exercise (Buono and Maly, 1996) and horses at exercise (Erickson et al., 1995) would mean that maximally exercising humans reach maximal acinar efficiency whereas horses do not (it may be that trained and motivated athletes can produce a ventilatory pattern closer to the maximum possible than horses in whom motivation for maximal exercise is uncontrollable).

In the presence of helium-related acinar unscreening, the fall in AaO_2 automatically comes with an increased CO_2 clearance. Indeed, in the study by Siddappa et al. (2003), $PaCO_2$ decreased as a function of helium concentration in the inhaled gas mixture, even though ventilation remains constant.

Finally, it should be noted that the need for an adequate diffusion–perfusion matching (see earlier) is less important in the case of helium–oxygen than in the case of air, because of the lower oxygen partial pressure heterogeneity. This could be a useful feature in certain pathological situations where abnormalities of the structure and function of the pulmonary vasculature compromise hypoxic vasoconstriction. Conversely, under SF_6–O_2, diffusion–perfusion matching is crucial for hemoglobin saturation.

5. Conclusions

The effects of diffusional screening in the human pulmonary acinus have been studied numerically using a coarse-graining scheme inspired from a classical procedure in statistical physics. Lacking direct experimental measurements of oxygen partial pressure in the intra-acinar airways, the numerical study of such processes is the only approach available. Of course, the accuracy of the results presented in this paper is limited by the fact that oxygen–hemoglobin binding is treated in a simplified manner and that the convection–diffusion transition is considered as abrupt at the entry of the subacinus. A rapid quantitative evaluation (Felici, 2003) shows that these two phenomena would weakly affect the efficiency values computed in our model, and would not change the general consequences of the screening phenomenon.

We have shown that the acinus efficiency is determined by its branching pattern only. It is therefore possible to perform simulations on simplified tree-like lattices designed on the acinus branching pattern. Random walk simulations on such lattices give the same quantitative result as direct numerical computation of the solution of the diffusion equation in the corresponding 3D geometries. This approach allows one to compute the efficiency of real human acini much more easily.

The net result is that, at rest, the efficiency of the human acinus is of order 30–40%. This is because the partial pressure distribution in the subacinus is not homogeneous. It decreases from the entry to the deeper regions, whereas carbon dioxide partial pressure is rather high and homogeneous everywhere except at the entry. This allows a reinterpretation of the notion of an uniform alveolar gas as being really a space average of an inhomogeneous mixture. One should stress that the existence of this inhomogeneity is *not* the consequence of an insufficient diffusion velocity during inspiration. Remarkably, the same theoretical frame applies quantitatively to both oxygen uptake and carbon dioxide clearance. It permits to predict, without any adjustable parameter, the value of the partial pressure of oxygen in venous blood from the partial pressure of CO_2.

The results of several experimental observations on breathing different respiratory gases (Heliox®, air and O_2–SF_6) are compatible with, or explained by the existence of screening which depends directly on the value of the diffusivity of oxygen in these gases. Note that the de-screening effect of Heliox® could give a hint of why it may help patients, although it contains *less* oxygen than pure oxygen. In fact, breathing pure oxygen increases the oxygen uptake but does not help carbon dioxide clearance whereas, for Heliox®, the acinus efficiency is increased for *both* oxygen uptake and carbon dioxide clearance. Again, the notion of uniform partial pressures gives only an average view of the system, which cannot explain such phenomena as the de-screening effects due to larger diffusivities of both oxygen and carbon dioxide in Heliox®. From a therapeutic point of view, these de-screening effects of helium–oxygen would add to the mechanical benefits related to the lower gas viscosity.

One can also envisage the manipulation of diffusional screening towards improved delivery of exogenous substances (e.g. drugs, or gene vectors). If transported in helium–oxygen rather than in air, such substances would have access to a larger exchange surface, and would be more likely to reach the more distal respiratory cells (e.g. alveolar epithelial cells).

The fact that good quantitative results are obtained very rapidly through random walk simulations, is promising for the study of more complex features of the respiratory system. In particular, the simulation of detailed diffusion dynamics could be used in the interpretation of polarized helium magnetic resonance images of the lung in relation to normal or pathological morphology of the acinus.

Acknowledgements

The authors wish to thank J. Soares Andrade Jr. for fruitful discussions and M. Guéron for his reviewing of the manuscript. They also are deeply grateful to H. Kitaoka for providing her acinus generating code, and to E.R. Weibel for providing experimental data.

References

Buono, M.J., Maly, R., 1996. Augmented hyperventilation via normoxic helium breathing does not prevent exercise-induced hypoxemia. Can. J. Appl. Physiol. 21, 264–270.

Dutrieue, B., Vanholsbeeck, F., Verbank, S., Paiva, M., 2000. A human acinar structure for simulation of realistic alveolar plateau slopes. J. Appl. Physiol. 89, 1859–1867.

Elliott, A.R., Steffey, E.P., Jarvis, K.A., Marshall, B.E., 1991. Unilateral hypoxic pulmonary vasoconstriction in the dog, pony and miniature swine. Respir. Physiol. 85, 355–369.

Erickson, B.K., Seaman, J., Kubo, K., Hiraga, A., Kai, M., Yamaya, Y., Wagner, P.D., 1995. Hypoxic helium breathing does not reduce alveolar–arterial P_{O_2} difference in the horse. Respir. Physiol. 100, 253–260.

Fan, M., Wang, D.X., Zhu, Z.H., 1992. Alteration in hypoxic pulmonary vasoconstriction during hypothermia in dogs. J. Tongji Med. Univ. 12, 134–138.

Felici, M., Filoche, M., Sapoval, B., 2003. Diffusional screening in the human pulmonary acinus. J. Appl. Physiol. 94, 2010–2016.

Felici, M., 2003. Physique du transport diffusif de l'oxygene dans le poumon humain. Ph.D. thesis, Ecole Polytechnique, Palaiseau, France.

Felici, M., Filoche, M., Sapoval, B., 2004. Renormalized random walk study of the efficiency of the mammalian pulmonary acinus. Phys. Rev. Lett. 92, 068101.

Haefeli-Bleuer, B., Weibel, E., 1988. Morphometry of the human pulmonary acinus. Anat. Rec. 220, 401–414.

Heistad, D.D., Wheeler, R.C., 1972. Effect of carbon monoxide on reflex vasoconstriction in man. J. Appl. Physiol. 32, 7–11.

Jolliet, P., Watremez, C., Roeseler, J., Ngengiyumva, J.C., de Kock, M., Clerbaux, T., Tassaux, D., Reynaert, M., Detry, B., Liistro, G., 2003. Comparative effects of helium–oxygen and external positive end-expiratory pressure on respiratory mechanics, gas exchange, and ventilation–perfusion relationships in mechanically ventilated patients with chronic obstructive pulmonary disease. Intensive Care Med. 29, 1442–1450.

Keener, J., Sneyd, J., 1998. In: Marsden, J.E., Sirovich, L., Wiggins, S. (Eds.), Mathematical Physiology. Springer-Verlag, New York.

Kitaoka, H., Tamura, S., Takaki, R., 2000. A three dimensional model of the human pulmonary acinus. J. Appl. Physiol. 88, 2260–2268.

Osborne, D.R., Effmann, E.L., Hedlund, L.W., 1983. Postnatal growth and size of the pulmonary acinus and secondary lobule in man. Am. J. Roentgenol. 140, 449–454.

Paiva, M., Engel, L.A., 1985. Model analysis of intra-acinar gas exchange. Respir. Physiol. 62, 257–272.

Paiva, M., Engel, L.A., 1987. Theoretical studies of gas mixing and ventilation distribution in the lung. Physiol. Rev. 67, 750–796.

Reid, C., Prausnitz, J.M., Poling, B.E., 1987. The Properties of Gases and Liquids. McGraw-Hill, New York.

Sapoval, B., 1994. Transfer to and across irregular membranes modelled by fractal geometry. In: Nonnenmacher, T.F., Losa, G.A., Weibel, E.R. (Eds.), Fractals in Biology and Medicine. Birkhäuser-Verlag, Bâle.

Sapoval, B., Filoche, M., Weibel, E.R., 2001. Branched structures, acinus morphology and optimal design of mammalian lungs. In: Fleury, V., Gouyet, J.F., Leonetti, M. (Eds.), Branching in Nature. EDP Sciences/Springer Verlag, pp. 225–242.

Sapoval, B., Filoche, M., Weibel, E.R., 2002a. Smaller is better-but not too small: a physical scale for the design of the mammalian pulmonary acinus. Proc. Natl. Acad. Sci. U.S.A. 99, 10411–10416.

Sapoval, B., Weibel, E.R., Filoche, M., 2002b. Diffusion screening, acinus size and optimal design of mammalian lungs. In: Losa, G.A., Merlini, D., Nonnenmacher, T.F., Weibel, E.R. (Eds.), Fractals in Biology and Medicine. Birkhäuser-Verlag, Bâle, pp. 25–38.

Schaeffer, E.M., Pohlman, A., Morgan, S., Hall, J.B., 1999. Oxygenation in status asthmaticus improves during ventilation with helium–oxygen. Crit. Care Med. 27, 2666–2670.

Scheid, P., Piiper, J., 1980. Intrapulmonary gas mixing and stratification. Pulm. Gas Exch. 1, 87–130.

Siddappa, R., Dowhy, M.S., Rotta, A.T., Hernan, L.J., Heard, C.M., Fuhrman, B.P., 2003. Heliox enhances carbon dioxide clearance from lungs of normal rabbits during low bias flow oscillation. Pediatr. Crit. Care Med. 4, 89–93.

Tawhai, M.H., Hunter, P.J., 2001. Characterising respiratory airway gas mixing using a lumped parameter model of the pulmonary acinus. Respir. Physiol. 127, 241–248.

Von Euler, U.S., Liljestrand, G., 1946. Observations on the pulmonary arterial blood pressure in the cat. Acta Physiol. Scand. 12, 301–320.

Watson, J., Kamm, R.D., Burwen, D.R., Brown, R., Ingenito, E., Slutsky, A.S., 1987. Gas exchange during constant flow ventilation with different gases. Am. Rev. Respir. Dis. 136, 420–425.

Weibel, E.R., 1984. The Pathway for Oxygen. Harvard University Press, Cambridge MA.

Weibel, E.R., Federspiel, W.J., Fryder-Doffey, F., Hsia, C.C., Konig, M., Stalder-Navarro, V., Vock, R., 1993. Morphometric model for pulmonary diffusing capacity. I. Membrane diffusing capacity. Respir. Physiol. 93, 125–149.